ÉCOLE POLYTECHNIQUE
FÉDÉRALE DE LAUSANNE

Semester Project

Finite Element Modeling of Acoustic Shielding via Phononic Crystal structures

Author :

Clémentine Lipp

Supervisor:

Guillermo Villanueva
Andrea Lozzi

Due date:

10th June 2016

Contents

1 Abstract

Quality factor of Contour Mode Resonators (CMR) are mainly affected by energy losses due to acoustic waves leaving the resonator through the anchors[10]. An engineering of the anchors in order to create a periodic variation in the acoustic impedance of the material, structures known as Phononic Crystals (PnCs), can help improve the Q factor by reflecting part of the acoustic waves. During this project, FEM models have been validated for both 1D and 2D PnCs. The behavior of the band diagram and quantification of transmission has been studied for three different PnC geometries: circle, cross and square unit cell. Parameters such as unit cell size, filling factor, material composition, thickness and number of repetitions have been varied and comparisons between transmission graph and band diagram allowed to understand better the nature of the modes. It has been found that a linear approximation can predict with a good precision the position of the band gap as a function of the unit cell size. These studies have been done in order to select the best configuration for a future integration on the substrate of a CMR whose frequency range of operation is situated between 200MHz and 500 MHz. The results obtained report a better attenuation and broader peak of attenuation for a cross unit cell made out of AlN and an attenuation increasing linearly with the number of repetitions.

2 Introduction

The aim of this project is to improve the quality factor of a Contour Mode Resonator (CMR) made out of aluminium nitride that is being developed for future application in communication and sensing. It is known [10] that the main loss mechanism at play in CMRs in the range of frequency corresponding to communication and sensing is due to so called anchor losses. This loss mechanism is due to acoustic waves generated by the resonator's motion that leave the resonator by traveling through the anchors. Recent research has shown that structuring the supporting beams or the substrate of a resonator in a periodic fashion, structure also known as Phononic Crystal (PnC), can reflect acoustic waves and therefore significantly improve the quality factor of the resonator. However, this reflection happens only for certain range of frequencies, known as band gap. The location and thickness of the band gap depends on the resonances of the structure which are defined by multiple parameters like geometry of the irreducible unit cell, size, material properties, etc. This project aims at studying the behavior of the band gap in terms of frequency, thickness and attenuation for PnCs of selected geometries as a function of different parameters.

3 Theoretical background

3.1 Quality factor

The quality factor of a resonator can be defined as:

$$Q = \frac{f_{res}}{\Delta f}$$

Where f_{res} is the frequency of resonance and Δf is the full width at half maximum that defines the sharpness of the resonance peak (Fig. 1). In the case of use of the resonator

for telecommunication application and sensing, it is intuitive to understand that a very sharp peak is desirable in order to have a good selectivity.

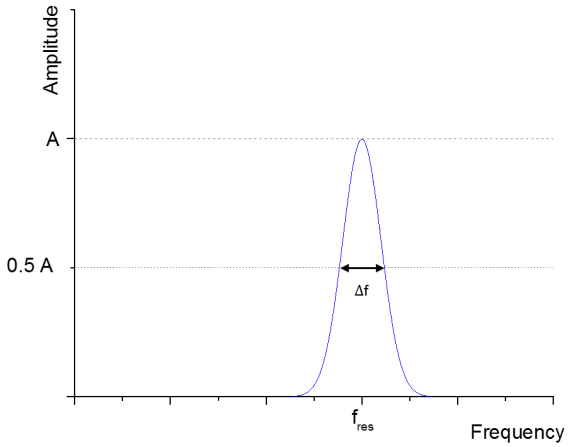

Figure 1: Full width at half maximum

The quality factor can also be defined as the ratio of the energy stored in a resonator over the energy dissipated during a cycle. It is thus an indicator of the energy losses of the resonator:

$$Q = 2\pi \cdot \frac{Energy\ stored}{Energy\ dissipated\ per\ cycle}$$

The quality factor is therefore decreasing as the energy losses increase. There are different loss mechanisms at play in a MEMS resonator. When expressing the total quality factor as a function of the independent loss mechanisms it becomes:

$$\frac{1}{Q_{tot}} = \frac{1}{Q_{air}} + \frac{1}{Q_{material}} + \frac{1}{Q_{anchor}}$$

It has been shown that CMR are not significantly affected by air damping due to the nature of its motion. Also, material losses are difficult to predict and to control. Therefore, the major loss mechanism between 200 and 500 MHz that can be minimized is the anchor losses [10].
Anchor losses are due to acoustic waves generated inside the material by the resonator's vibration and that travel through the anchor and leave the resonator with a nearly null probability of going back to the resonator (Fig. 2).
An increasing interest has been brought during the past twenty years to structures called Phononic Crystals (PnC) amongst others because they can prevent acoustic waves from leaving the resonator when integrated to a chip.

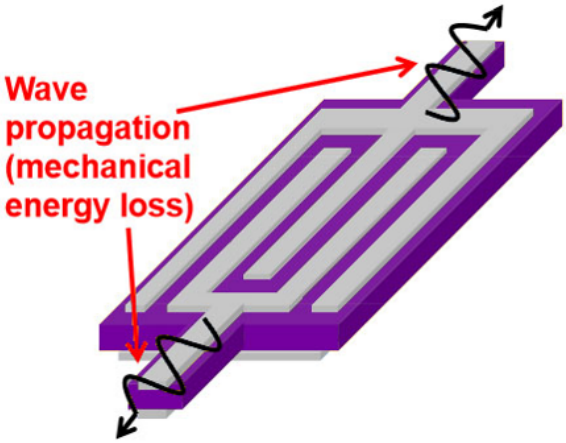

Figure 2: Anchor loss in a CMR

3.2 Introduction to Phononic Crystal

A phononic crystal is a periodic arrangement of alternatively low and high acoustic impedance materials. A simplified version of a PnC that can help understanding their working principle is the Bragg mirror, that is a superposition of layers of alternatively low and high impedance material. As a result of the acoustic impedance mismatch ΔZ, reflection and transmission happen at the boundaries following the rule:

$$R = \left(\frac{\Delta Z}{Z_1 + Z_2} \right)^2$$

and:

$$T = 1 - R$$

Therefore, the larger the acoustic impedance mismatch the larger the fraction of energy being reflected. Furthermore, constructive interference happen between the reflected waves when the thicknesses of the layers are set to be one quarter of the effective wavelength in the respective materials, leading to a very small fraction of energy being transmitted through the structure at this specific frequency.

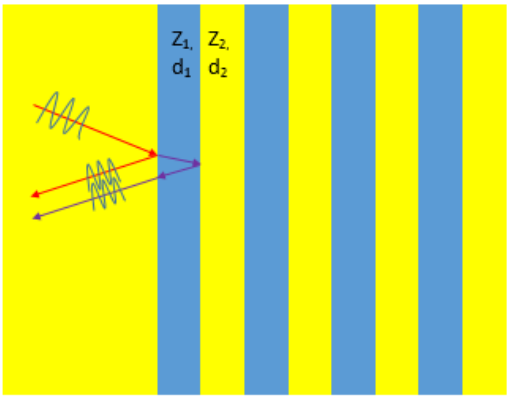

Figure 3: Illustration of a simplified version of a PnC: the Bragg mirror. Constructive interference happens between the reflected waves at normal incidence for $d_1 = \frac{\lambda}{4 \cdot n_1}$ and $d_2 = \frac{\lambda}{4 \cdot n_2}$

In the case of MEMS resonators, it would be very complex to create layers of two different materials at the anchor in terms of manufacturing process. Furthermore the constructive interference would happen for different wavelengths depending on the direction of propagation. As the anchor acts as a point source of sharp frequency distribution, the reflection would therefore probably not be optimal. A simple way of integrating a periodic variation in the acoustic impedance is to create periodic patterns using photolithography. The low acoustic impedance material is therefore the resonator's material itself whereas the second material is air. As this latter has a very high acoustic impedance, the acoustic impedance mismatch is large and thus enhances the reflectivity. The pattern created can be either integrated on the supporting beams of the resonator (Fig.4b), or on the substrate (Fig.4a). The first method has the advantage of being more compact and to be released faster than the second one, but it might also induce a weakening of the structure.

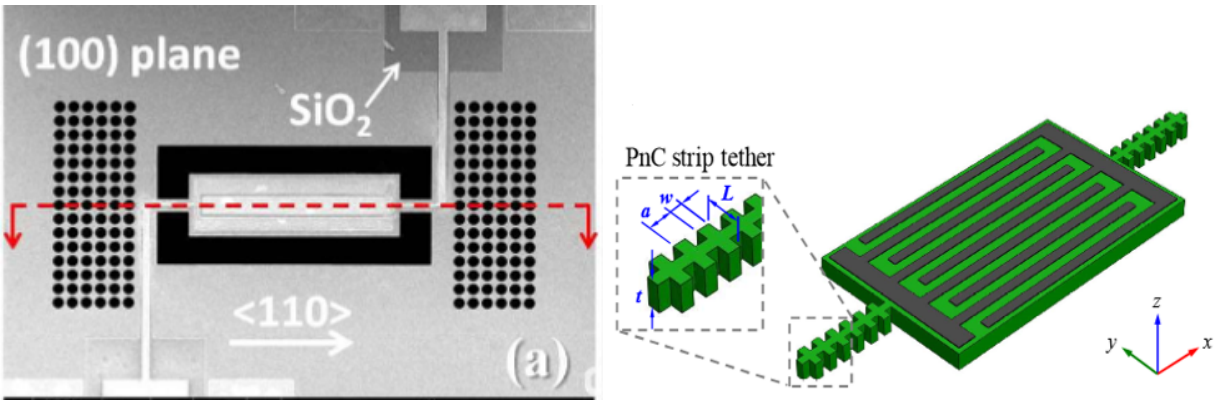

(a) (b)

Figure 4: Examples of PnC integration: a) 2D PnC located on the substrate designed by Zhu & Lee [13] b) 1D PnC integrated on the supporting beams designed by Lin et al. [9]

3.3 Band diagram and FEM model

3.3.1 Procedure

A commercial FEM software was used to study the frequency behavior of the PnCs. The first step is to reduce the structure to an irreducible unit cell. The Floquet conditions are then set on the faces in the direction of repetition of the structure (Fig. 5). This condition is therefore applied only on two faces in the case of a 1D PnC and on four faces for a 2D PnC. This condition imposes that there is an infinite number of repetitions of the unit cell in these directions: the modes allowed to travell in such a structure are its resonant modes. This is thus an approximation of the real structure but it allows to assess potential stop bands created by the structure.

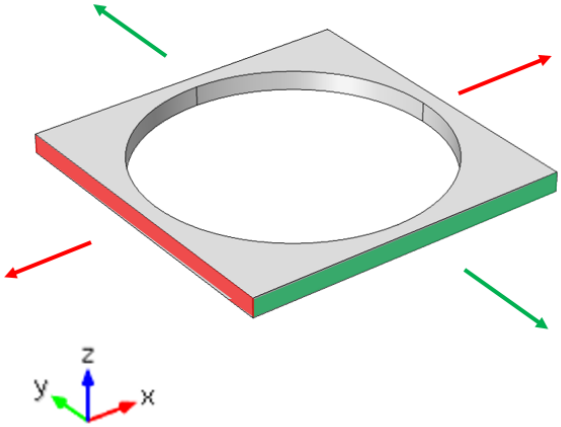

Figure 5: Floquet conditions applied to a circle unit cell: the condition applied on the red faces implies an infinite number of repetition in the x direction and the condition applied on the green faces implies an infinite number of repetition in the y direction

In this work, it was assumed that studying the behavior of the structure for a wave vector k swept from the Γ point of the reciprocal space to the X point for a 1D PnC and from the Γ point to the X point, from the X point to the M point and finally from the M point to the Γ point for a 2D PnC is sufficient to span enough of the modes for a good modelization. This practically means that for the Γ to X sweep the x component of the k vector k_x will range from 0 to $\frac{\pi}{a}$, a being the size of the irreducible unit cell, while the y component k_y will be set to 0. Then for the X to M simulation k_x will have constant value of $\frac{\pi}{a}$ while k_y will be swept from 0 to $\frac{\pi}{a}$, and for the M to Γ step both components will be swept simultaneously from $\frac{\pi}{a}$ to 0 until k reaches the Γ point. These steps are illustrated by Figure 6.

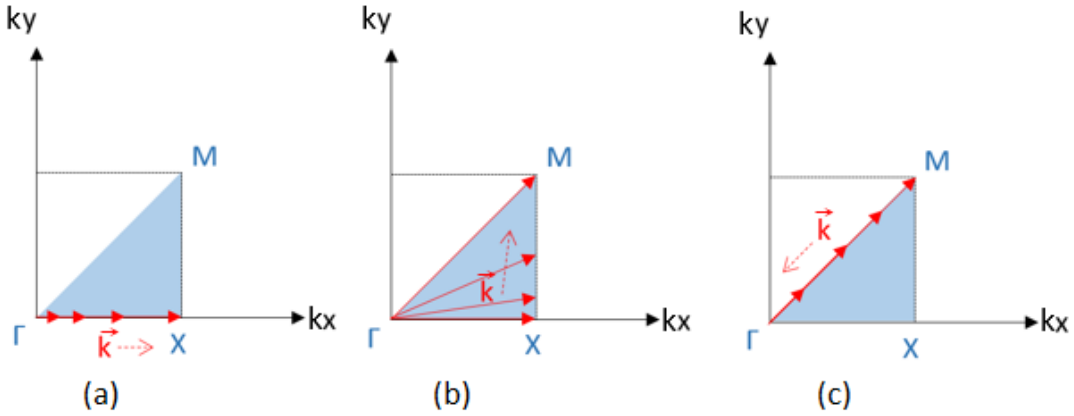

Figure 6: Illustration of the **k** vector sweep in the first Brillouin zone: a) Γ to X b) X to M c) M to Γ

The band diagram obtained by Finite Element Method relates the frequency of the resonant modes for each value of the wave vector k. The dispersion relation for waves traveling in an homogeneous medium is given by the following relation:

$$\omega = c \cdot k$$

where c is the velocity of the wave in the medium and ω is the angular frequency. The velocity is given by $c = \sqrt{\frac{E}{\rho}}$ for longitudinal waves and $c = \sqrt{\frac{G}{\rho}}$ for shear waves for example with E and G being the Young modulus and the shear modulus respectively of the material. In the case of PnC, the material is not homogeneous but the properties defining the material follow a periodic variation. The previous dispersion relation is therefore not valid. The analytical expression of the dispersion relation is much more complicated but is graphically given by the band diagram. As seen on the Γ to X and M to Γ parts of the band diagram of Figure 7, the frequency is no more linearly dependent on the modulus of the wave vector k for the same direction of propagation of the wave.

3.3.2 Band gap

A *complete* band gap is a range of frequencies where no resonant mode is found on the band diagram. This physically means that at these frequencies acoustic waves are not allowed to travel in the structure of infinite number of repetitions. On the example of Figure 7 it is represented by the black shaded area.
A *deaf* band gap is a range of frequencies where the only resonant modes allowed to propagate at these frequencies are not likely to be excited by the resonator's motion. In literature, it is often assumed that transverse or shear modes are not likely to be excited by Lamb wave resonators and CMRs. On the example of Figure 7 it is represented by the red shaded area.

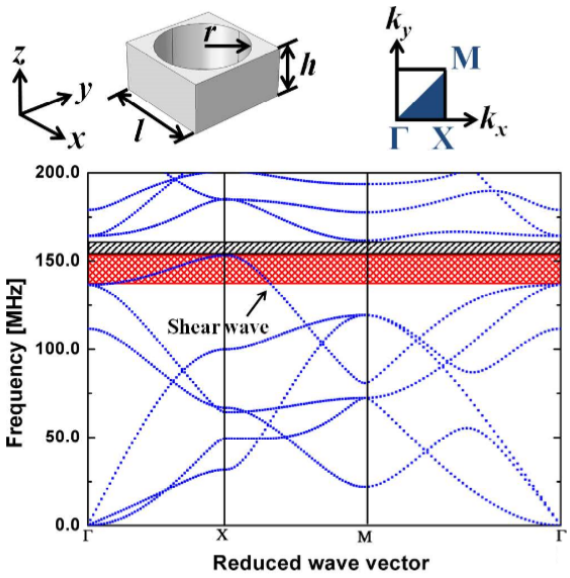

Figure 7: Example of band diagram obtained for a circle unit cell as obtained by Zhu & Lee [13]

4 State of the art

4.1 *Phononic Crystals, Fundamentals and Application*, Khelif & Adibi [1]

This book summarizes the state of the research in the field of PnCs and presents the background theory needed to explain the phenomena at play in such structures. This very complete work first describes the analytical methods that can be used in order to solve the non linear problem of waves equations in periodic media. One can point out the dispersion relation in the case of a one dimensional phononic crystal:

$$cos(kd) = cos\left(\frac{\omega a}{c_a}\right) cos\left(\frac{\omega b}{c_b}\right) - \frac{1}{2}\left(\frac{z_b}{z_a} + \frac{z_a}{z_b}\right) sin\left(\frac{\omega a}{c_a}\right) sin\left(\frac{\omega b}{c_b}\right) \quad (1)$$

where a and b are the respective thicknesses of the layers of the two different materials, $d = a + b$ is the size of the unit cell, c_a and c_b are the respective velocities of the waves in the two different materials (dependent on the mode type), $z_a = \rho_a c_a$ and $z_b = \rho_b c_b$ are the acoustic impedances of the different materials (therefore also depending on the type of mode). This equation relates the wave vector k with the $\omega_n(k)$ that satisfy Equation 1.

In the case where the right hand side of the equation is larger than unity (the necessary but not sufficient condition is a large enough difference in the acoustic impedances), there is no solution to this equation for wave vector laying in the Brillouin zone ($|k| < \frac{\pi}{d}$). The range of frequencies, if it exists, where no k is able to satisfy Equation 1 will therefore define the band gap. In the case where $kd, \frac{\omega a}{c_a}, \frac{\omega_b}{c_b} \ll 1$ the equation can be approximated to the one defining an homogeneous media:

$$\omega = c_{eff} \cdot k \quad (2)$$

Which means that the periodic structure behaves like an homogeneous media in which the waves travel at a speed c_{eff}.
In the case of a 2D PnC, Equation 1 becomes much more complex. In order to see a band gap open in a 2D PnC constituted of a *matrix* element material and an *inclusion* material, two main requirements must be fulfilled. The first is that there must be a significant difference in the materials properties such as speed of sound and density in the two materials forming the structure. The second is that the filling factor, defined as

$$f = \frac{Inclusion\ element\ area}{Unit\ cell\ area}$$

must have a minimum value in order to see a band gap opening.
Furthermore, the position of the band gap is defined by the ratio of effective sound velocity in the media over size of the periodic unit cell.
A description of the band gap created by a Si 2D PnC slab structure with square-lattice of circle unit cell is given as a function of the ratios $\frac{r}{a}$ and $\frac{d}{a}$, r, a and d beings the radius of the hole inclusion, the unit cell size and the slab thickness respectively. As it can be observed in the graphs shown in Figure 8, there is an optimum ratio $\frac{d}{a}$ around 0.55 that maximizes the band gap thickness (Fig. 8a) and that the band gap thickness increases with the ratio $\frac{r}{a}$ (Fig. 8b).

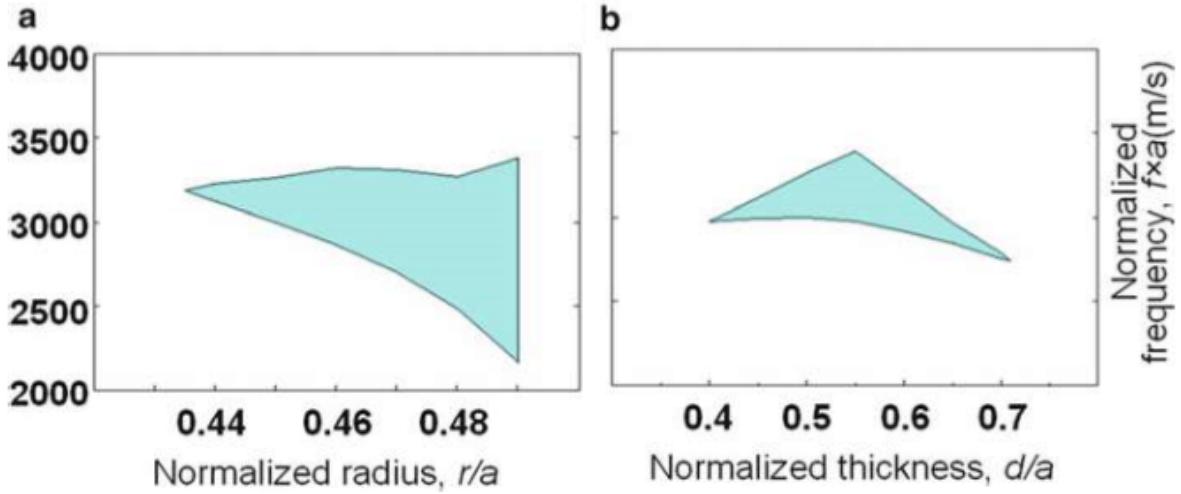

(a) (b)

Figure 8: Band gap evolution for a Si 2D PnC slab structure with square-lattice of circle unit cell [1]: a) $\frac{d}{a} = 0.5$, the band gap thickness increases with the ratio $\frac{r}{a}$
b) $\frac{r}{a} = 0.45$, an optimum ratio $\frac{d}{a}$ around 0.55 maximizes the band gap thickness

In the case of this project,t the slab thickness of the CMR is fixed to $1\mu m$. As the wavelength of the waves excited by the CMR are in the range of the tens of microns, the ratio $\frac{d}{a}$ corresponding is not in the scope of the graph of Figure 8b, but another opening of a band gap may happen for lower value of the ratio.
An interesting point mentioned by this book is that the arrangement of the geometry plays a role in the band gap opening. For example the band diagram obtained for a

similar structure as the previous case but with circles arranged in an hexagonal fashion shows a much larger band gap than for the square lattice case, as illustrated by Figure 9.

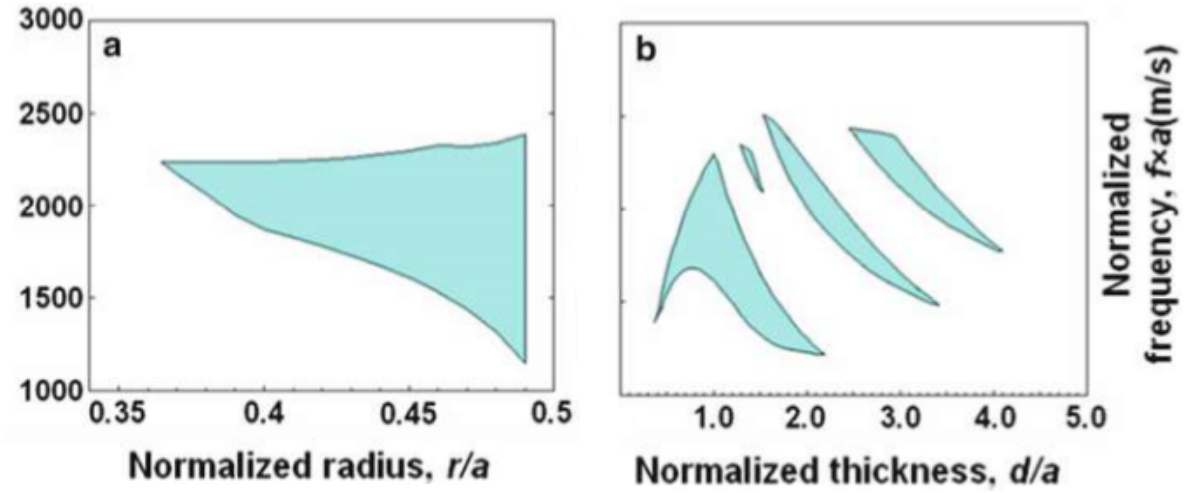

(a) (b)

Figure 9: Band gap evolution for a Si 2D PnC slab structure with circles arranged in an hexagonal fashion [1]: a) $\frac{d}{a} = 1$ b) $\frac{r}{a} = 0.45$

In this case the ratio $\frac{d}{a}$ concerned in this project ($\frac{d}{a} \approx 0.06$) is covered by the scope of the graph but no band gap seems to be associated for $\frac{d}{a} < 0.3$. However a larger filling factor could potentially lead to an opening of a band gap for low values of the ratio.

4.2 Microscale inverse acoustic band gap structure in aluminum nitride, Kuo et al. [8]

This paper brings a solution to the problem caused by the requirement of common PnCs to have a ratio $\frac{d}{a} \approx 1$ whereas electroacoustic devices usually require a film thickness of $1 - 2\mu m$. Kuo et al. demonstrates the properties of an Inverse Acoustic Band Gap (IABG) structure. This class of PnC stands out because of the matrix material being the high acoustic impedance material (air in this case) and the inclusion being formed by the low acoustic impedance material (AlN in this case). The unit cell is $8.6\mu m$ long and is made out of a $2\mu m$ thick AlN layer sandwiched between two $200nm$ thick Pt layers as shown on Figure 10. The measurements performed with transducers on the structure demonstrate the presence of a band gap ranging from 185 MHz to 240MHz with a ratio $\frac{d}{a} = 0.23$, which is larger than the complete band gap predicted by the band diagram because of the nature of the modes excited by the transducers.

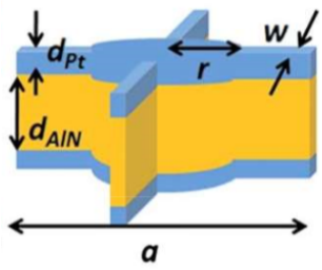

Figure 10: Unit cell of the structure studied by Kuo et al. [8] with $a = 8.6\mu m, r = 3.3\mu m, w = 1\mu m, d_{AlN} = 2\mu m, d_{Pt} = 200nm$

4.3 1 GHz phononic band gap structure in air/aluminum nitride for symmetric lamb waves, Kuo & Piazza [6]

This work reports a large acoustic band gap ranging from 860MHz to 1.2GHz created by an X-shape unit cell as illustrated by Figure 11. This unit cell shape could therefore meet the high frequency range of operation of telecommunication while using a minimum feature size larger than what a conventional circle unit cell would require in order to have a band gap in this range of frequencies. Indeed the nature of the air inclusion is such that a band gap opens into higher order modes. The round shape of the cross is introduced in order to take into account the lithography limit and they report an up shift in the band gap frequency with an increase in the rounding of the edges. They also introduce a novel technique of measuring the magnitude of acoustic rejection provided by the structure using the commercial software COMSOL ®. The measured band gap is larger than the complete band gap predicted by the band diagram because of the symmetric lamb-wave nature of the modes generated by the transducers.

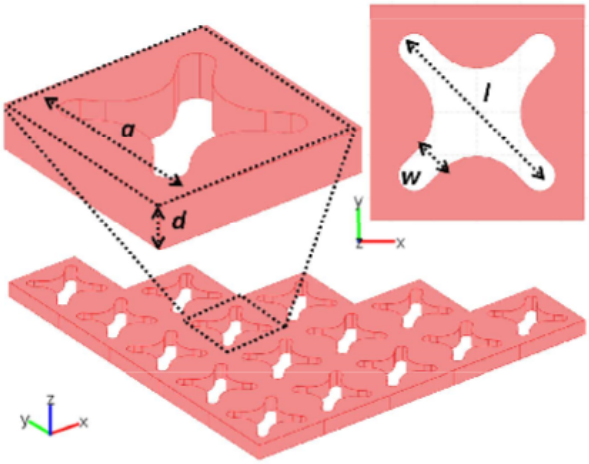

Figure 11: Unit cell and array of the structure studied by Kuo et al. [6] with $a = 5\mu m$, $l = 4.2\mu m$, $w = 750nm$ and $d = 1\mu m$

4.4 Fractal phononic crystals in aluminum nitride: An approach to ultra high frequency band gaps, Kuo & Piazza [7]

This paper introduces a novel type of geometry that is able to reduce the scattering length of the phonons while keeping the unit cell size. This geometry enables the operation of the PnC to higher modes and up shifts the band gap frequency into the high frequency range while keeping a reasonable minimum feature size, avoiding a drastic miniaturization of the PnC dimensions. A unit cell size of $5\mu m$ using this geometry results in the formation of two wide band gaps between 850MHz and 950MHz and between 1.05MHz and 1.15GHz.

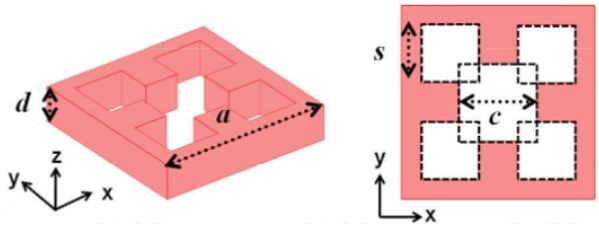

Figure 12: Fractal unit cell studied by Kuo et al.[6], the four smaller squares acting as phonons scatterers with $a = 5\mu m, c = 2\mu m, s = 1.5\mu m$ and a thickness of $1\mu m$

4.5 AlN piezoelectric on silicon MEMS resonator with boosted Q using planar patterned phononic crystal on anchors, Zhu & Lee [13]

The evolution of the quality factor of a resonator whose anchor (Si) is structured with periodic circular air inclusions is reported as a function of the radius of the circle. They find an increase in both the measured and the simulated quality factor for a larger air inclusion area, which is coherent which what Abdelkrim & Adibi reported [1]. They also find that a change in the radius impacts the location of the band gap.

4.6 Anchor Loss Reduction in AlN Lamb Wave Resonator Using Phononic Crystal Strip Tethers, Lin et al. [9]

The supporting beams of an AlN lamb wave resonator are structured in order to create a 1D PnC of cross shaped unit cell as seen on Figure 4b. They report the evolution of the complete band gaps found on the band diagram as a function of the supporting beam width w obtained by FEM simulation and hence show that the respective positions can be tuned by modifying independently the different dimensions. A deaf band is also reported: the twisting resonant mode present in this frequency range is effectively not likely to carry energy for waves created by a lamb wave resonator. The complete band gap present between 562 and 624MHz can therefore be further extended by a deaf band gap present between 521 and 562MHz. A small complete band gap is located between 198 and 229MHz.

4.7 Conclusion

A very large range of geometries has been studied in the PnC community and many are promising for band gap creation in the frequency range of operation of the CMR of interest for this project(200 to 500MHz). The geometries selected are presented below.

4.7.1 Circle unit cell

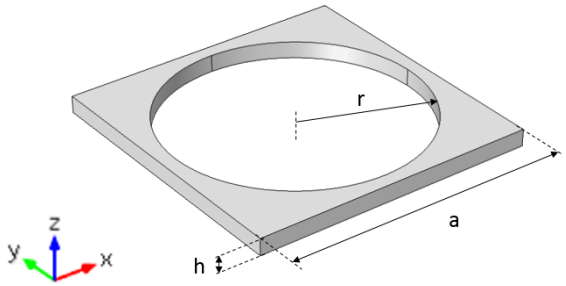

Figure 13: Circle unit cell

This classical geometry has been selected to be studied in this project because it is known to be associated with band gaps [1] [13]. Even though AlN layer induces a small value of the ratio $\frac{d}{a}$ and hence may not be optimum for the creation of a large complete band gap, it will enable to compare results with those found in literature and thus help understand the behavior of such structures.

4.7.2 Cross unit cell

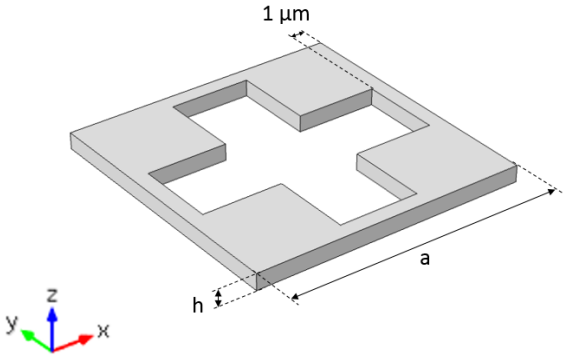

Figure 14: Cross unit cell: the cross is made out of the juxtaposition of five squares of the same size

After the work done by Kuo et al. [7] [6] this geometry seemed to be promising because of the low scattering length and because of the sub repetitions inside the unit cell (the cross

is made out of the juxtaposition of five squares of the same size) that could potentially broaden the band gap.

4.7.3 Square

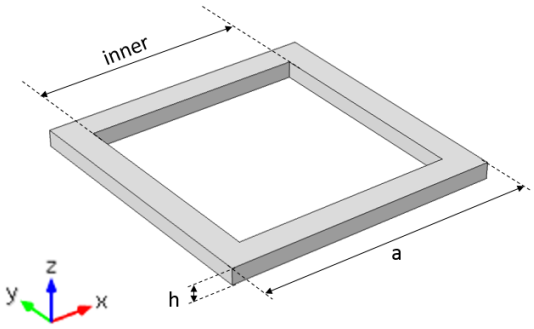

Figure 15: Square unit cell

This more unconventional geometry was studied because the effective acoustic impedance of a unit cell's cross section experience a very sharp increase. This fact seemed promising as it increases the reflection at the boundaries and thus it could potentially increase the whole structure's reflectivity.

5 Model Validation

The first step was to validate the model built using a commercial software. This was done by reproducing a structure studied by a paper and comparing the band diagram obtained with the one presented in the paper. Since the interest was brought on 2D aluminum nitride structures and that the only PnC using a simple geometry made out of AlN that was found in literature was a 1D PnC, a second validation was done for a 2D PnC made out of Si.
For all the simulations done in this work the materials were set as isotropic and the mesh used was a free tetragonal mesh built on the surface and swept in the thickness direction by steps of $1\mu m$.

5.1 1D AlN cross shape unit cell

The first structure reproduced was the one studied by Lin et al. [9]. They structured the supporting beams of a resonator made out of AlN with a cross shaped unit-cell as illustrated by Figure 16. The band diagram they obtained in comparison with the band diagram obtained in this work after simulation is shown in Figure 17.
The Young modulus and Poisson ratio used were extracted from the compliance matrix of AlN given by the FEM software and are respectively: $E = 349.8GPa$ and $\nu = 0.3$.

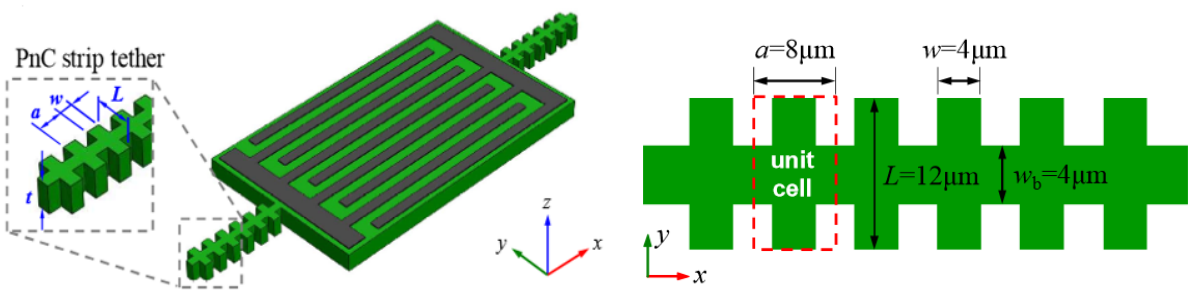

(a) (b)

Figure 16: 1D AlN PnC studied by Lin et al.[9] with a thickness of $4\mu m$

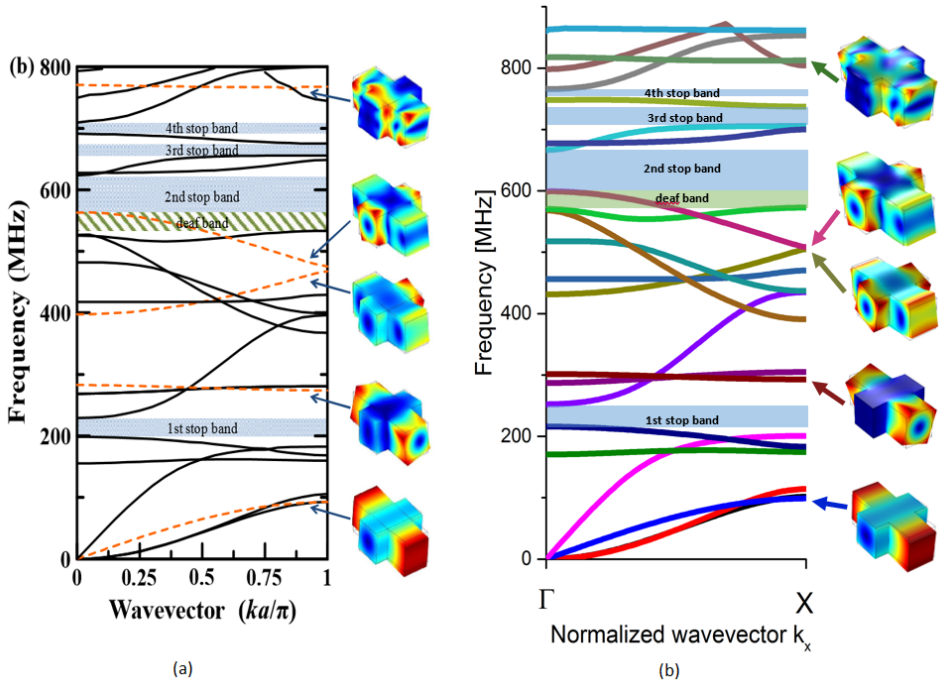

Figure 17: a) band diagram obtained by Lin et al.[9] b) band diagram obtained in this work

What has been observed from this comparison is that the global shape of the band diagram is conserved and that the same mode shapes are found for the same bands. However the band diagram obtained in this work is "expanded" compared to the one obtained by Lin et al.: the bands are found at the same frequencies in the low frequency range but at the frequency is increased the bands are located at higher frequencies than the ones from Lin et al. This can be explained by a difference in the Young modulus and Poisson ratio used. Indeed, it has been observed that a change in these parameters had the effect to "compress" or "expand" the band diagram. Since Lin et al. did not mention in their work the value of the Young modulus and Poisson ratio used, it was assumed that extracting it from the compliance matrix of the material given by the FEM software would lead to a sufficiently realistic value.

5.2 2D Si circle unit cell

The 2D PnC reproduced was found in the work of Zhu & Lee [13]. The PnC is located externally on the anchors as illustrated by Figure 18. The comparison of the two band diagrams obtained is shown on Figure 19. The Young modulus and Poisson ratio used were given by the FEM software and are respectively: $E = 170GPa$ and $\nu = 0.3$.

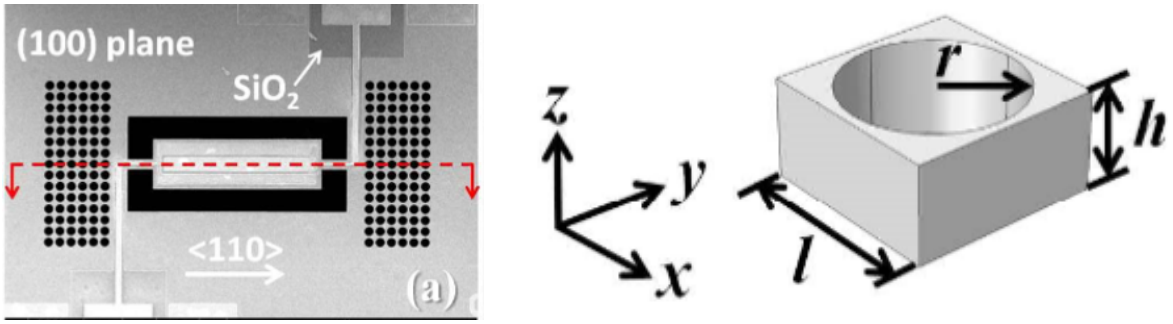

(a) (b)

Figure 18: 2D Si PnC studied by Zhu & Lee [13] a) integration of the PnC b) unit cell's dimensions: $l = 20\mu m, h = 10\mu m, r = 9\mu m$

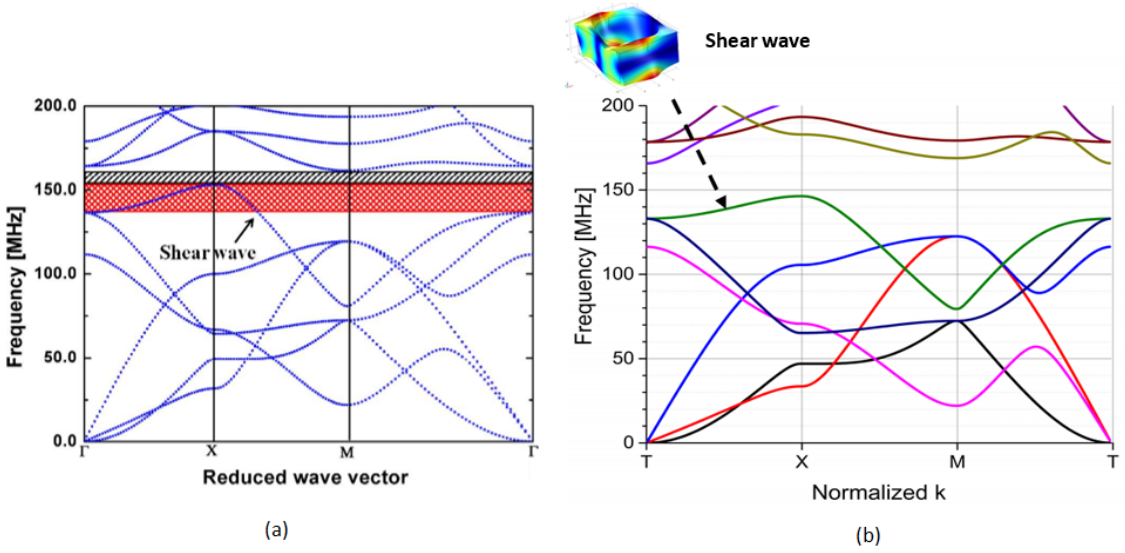

Figure 19: a) band diagram obtained by Zhu & Lee [13] b) band diagram obtained in this work

In this case the global shape is also conserved for bands situated under the band gap, with a small down shift compared to Zhu & Lee that can be explained by a difference in the Young modulus. The shear wave is also found for the same band. However when looking above the band gap the bands are not situated at the same position with respect to another: the purple and dark yellow curve are shifted downward compared to the red ones. This may be explained by the fact that Zhu & Lee did consider the material as anisotropic with a Poisson ratio dependent on the orientation. However they don't give the exact value of the Poisson ratio and the Young modulus.

In conclusion the band diagrams are similar enough to be able to validate the model used. Discrepancies can be explained by different values of Poisson ratio and Young modulus.

6 Band diagram

As seen in literature [1] [7] [13][9], multiple parameters have an effect on the shape of the band diagram. To get a better understanding of the dependences, the following sets of simulations were performed.

6.1 Effect of unit cell size

The first set of simulation was performed on circle unit cell and aimed at defining the role of unit cell size.
The parameter $h = 1\mu m$ was set by the fabrication process, the filling factor defined as $f = \frac{\pi r^2}{a^2}$ was kept constant to a value of $f = 0.64$. This value has been chosen from the work done by Zhu & Lee [13] in order to be able to compare with the band diagram they obtained. The unit cell size took the values: $a = 5, 10, 15, 16, 17, 18, 20\ \mu m$.

The first thing that can be observed from Figure 20 is that the density of modes per frequency is increasing as the unit cell size increases. The band diagram seems to be compressed for larger values of unit cell size and each band covers a smaller range of frequency. A second observation is that there is no band gap in this range of frequencies for unit cell sizes $a = 5\mu m$ and $a = 10\mu m$ but one exists for $a = 15\mu m$ and $a = 20\mu m$. This is due to the fact that the ratio $\frac{h}{a}$ is also varying since h is fixed. If the ratio had been kept constant, bands would probably have been positioned at the same place with respect to each other and the change in unit cell size would have just "shrunk' or "expanded" the band diagram.
The nature of the bands was studied for the bands adjacent to the complete band gap in order to determine if this latter could be further extended to a deaf band gap. As it is common to do so in literature, it was assumed that transverse and torsional modes were not likely to be excited by the resonator's motion whereas longitudinal modes were. Figure 21 illustrates the band diagram obtained for $a = 17\mu m$ and the shape of the modes next to the complete band gap.

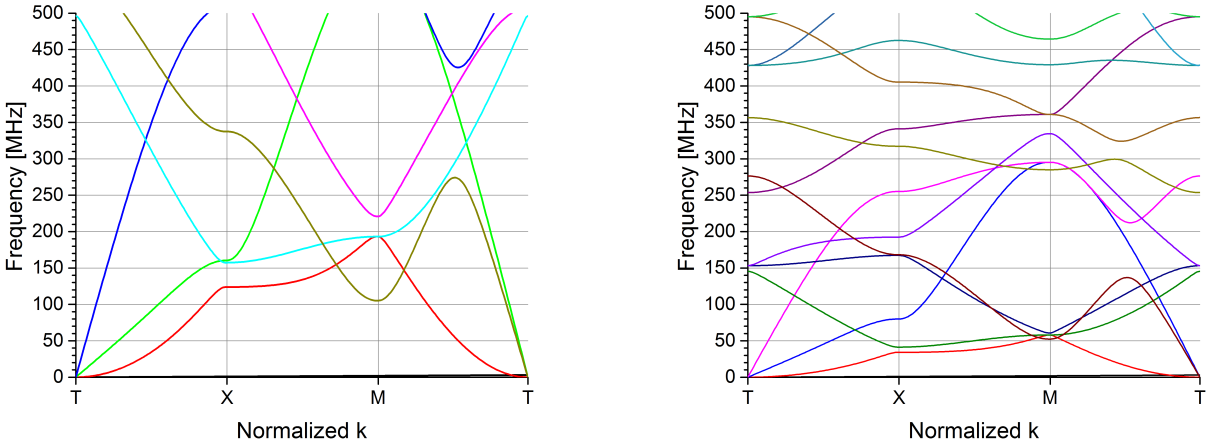

(a)

(b)

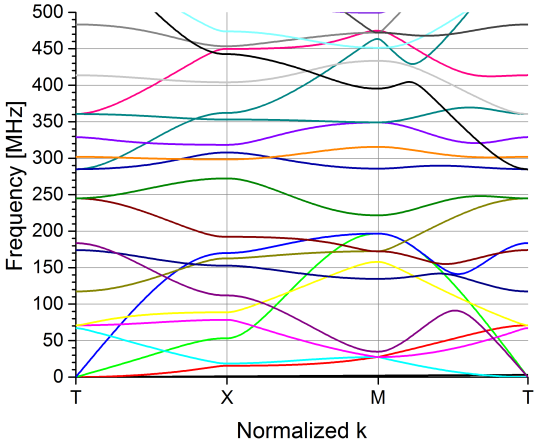

(c)

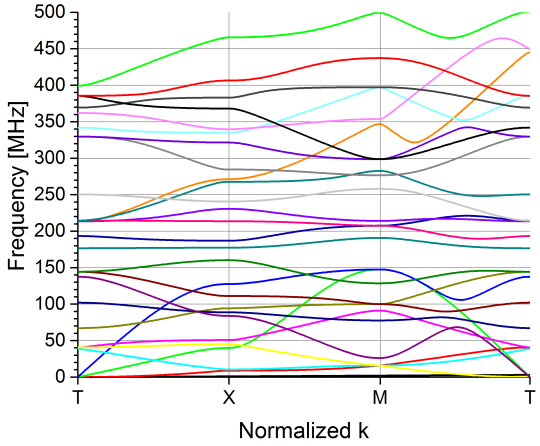

(d)

Figure 20: Band diagrams obtained for a circle unit cell with $h = 1\mu m, f = 0.64$ and variable unit cell size: the density of modes per frequency increases and each band covers a smaller range of frequency as the unit cell size increases a) $a = 5\mu m$ b) $a = 10\mu m$ c) $a = 15\mu m$ d) $a = 20\mu m$

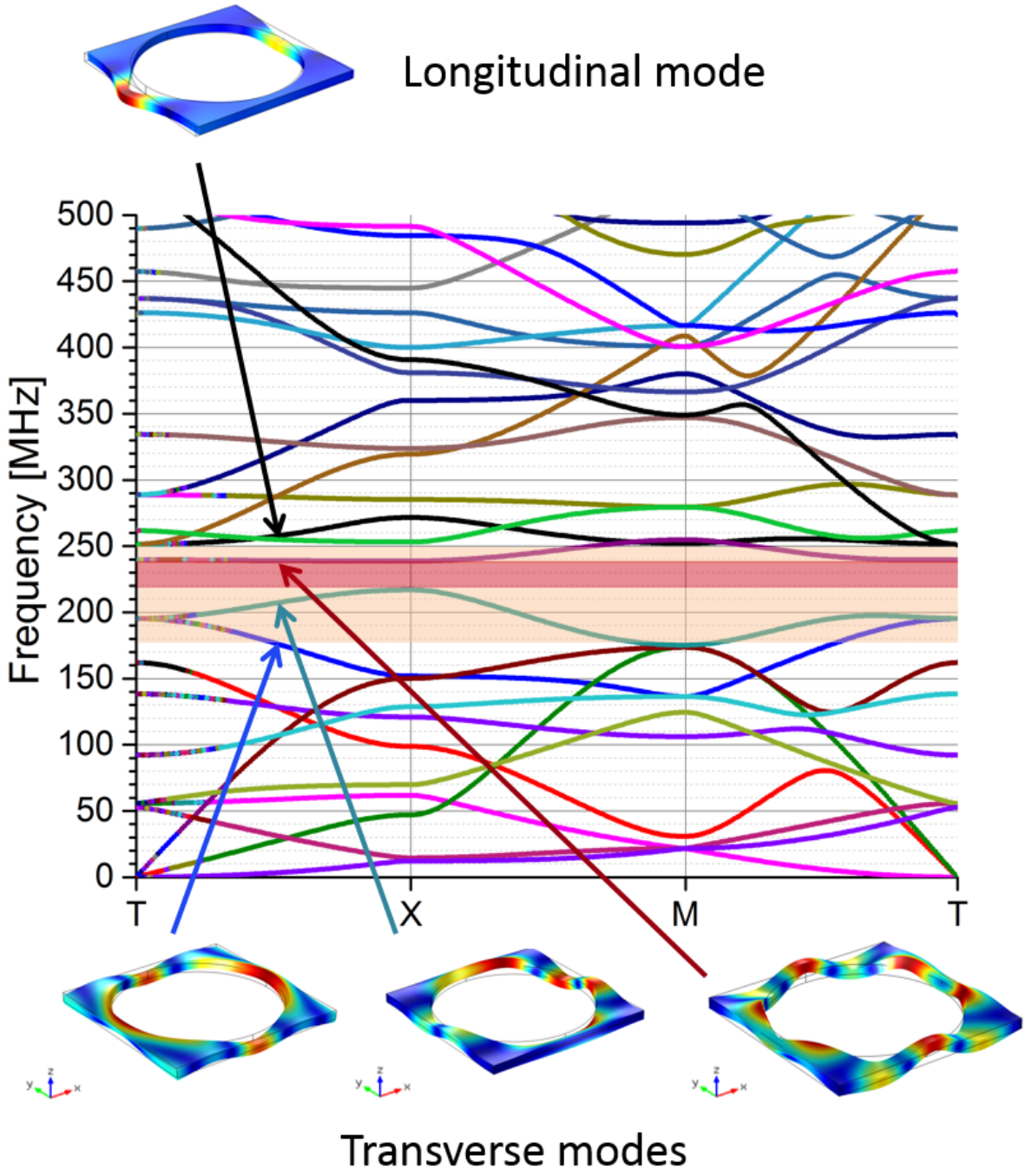

Figure 21: Band diagram and different mode shapes for a circle unit cell with $a = 17\mu m, h = 1\mu m, f = 0.64$: red area is the complete band gap, orange area is the supposed deaf band gap

This process was done for all the graphs obtained and the corresponding evolution of the complete and supposed deaf band gaps is shown on Figure 22.

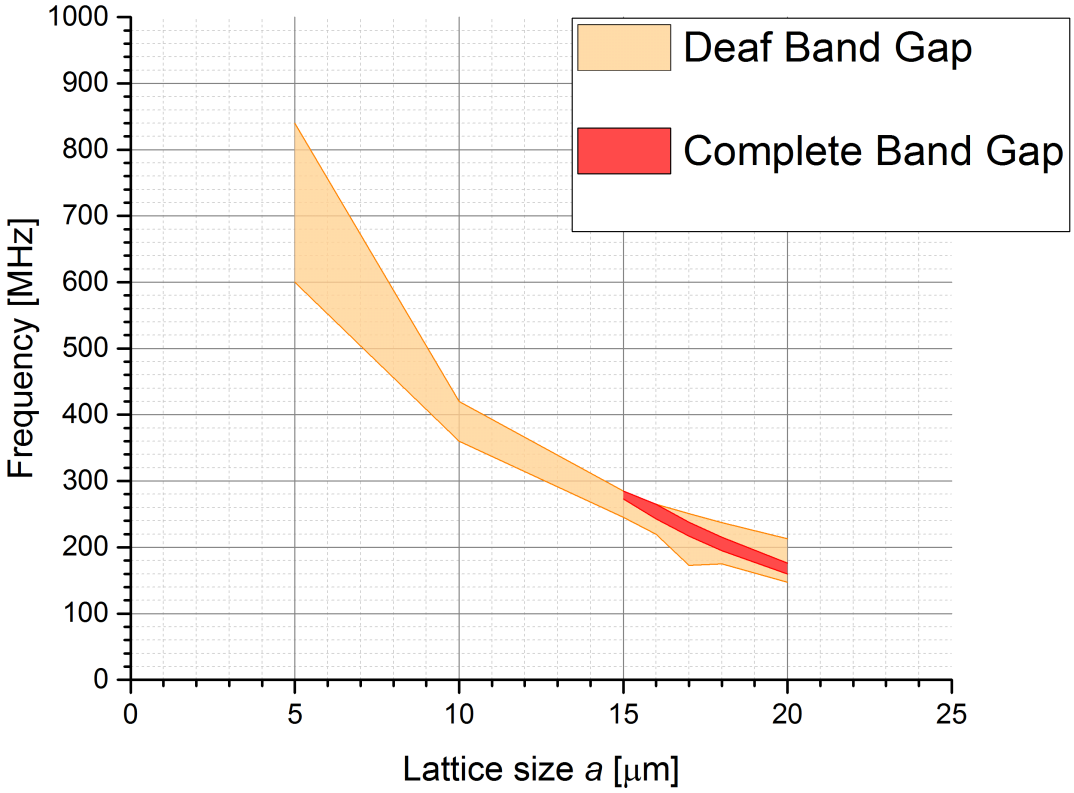

Figure 22: Evolution of the complete and supposed deaf band gaps as a function of the unit cell size for $f = 0.64$ and $h = 1\mu m$

The position of the complete and supposed deaf band gap lowers with an increase in the unit cell size. An interesting point that can be raised is that in the order of the tens of microns the behavior of the band gap can be well approximated by a linear interpolation. In order to target a specific band gap frequency, the band gap can be therefore situated for two different unit cell sizes and a linear interpolation approximation situates quite precisely the unit cell size required in order to have it centered on that specific frequency. This method has been further used for other geometries and has led to conclusive results.

6.2 Effect of material and thickness

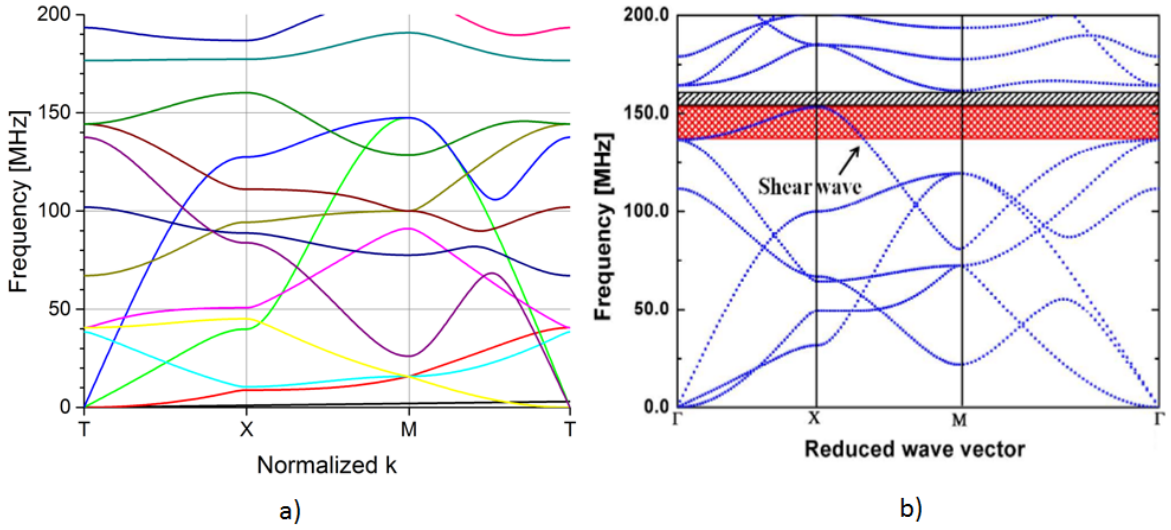

Figure 23: a) band diagram obtained for an AlN circle unit cell with $a = 20\ \mu m, h = 1\mu m, f = 0.64$ b) band diagram obtained by Zhu & Lee [13] for a Si circle unit cell $a = 20\mu m, h = 10\mu m, f = 0.64$

Figure 23 compares Figure 20d with the band diagram obtained for the same unit cell and circle size but with a thickness of $10\mu m$ and Si as material as obtained by Zhu & Lee. It can be observed that the band diagrams are very similar, but with noteworthy differences: the bands are up shifted in the case of the AlN unit cell. This can be explained by the fact that AlN has larger $\frac{E}{\rho}$ and $\frac{G}{\rho}$ ratios than Si which leads to larger wave velocity for both longitudinal and transverse modes in the structure and thus larger frequencies for the same mode and same wave vector when considering the linear approximation 2. Another interesting difference is the larger number of modes in the case of the AlN unit cell. When looking at the additional bands it can be noticed that these are actually transverse mode. Indeed the reduction by a factor ten in the layer thickness induces an easier propagation of z modes and new bands appear.

6.3 Effect of filling factor

The effect of the filling factor on the band diagram was studied by comparing the band diagram obtained with unit cells of lattice parameter $a = 17\mu m$, $h = 1\mu m$ and different filling factors $f = 0.64, 0.61, 0.50$.

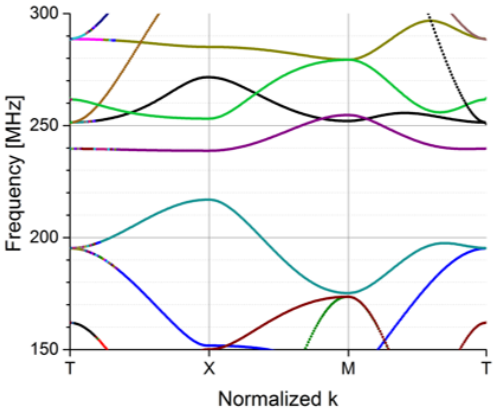

(a)

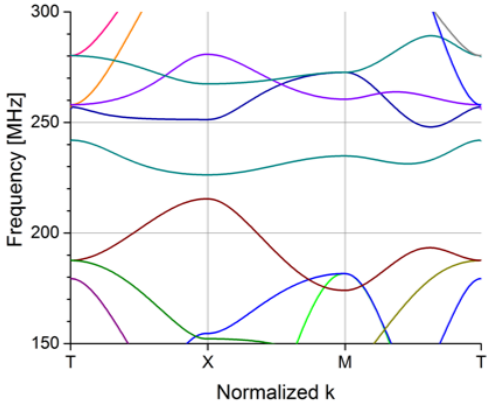

(b)

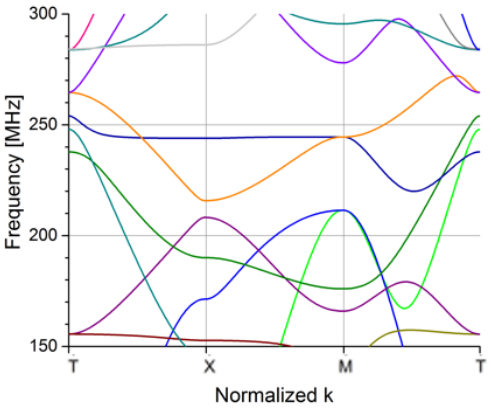

(c)

Figure 24: Zoom on the band gap for a circle unit cell with $a = 17\mu m, h = 1\mu m$: the band gap progressively closes as the filling factor decreases a) $f = 0.64$ b) $f = 0.61$ c) $f = 0.5$

The results found in literature [13] [1] is confirmed for this example: reducing the filling factor has the effect of closing the band gap if this latter exists. Here it is seen that a change in the filling factor impacts more specifically certain modes than others, which leads to their displacement toward the band gap.

6.4 Effect of the geometry

The band diagram of the three different geometries have been compared for the same unit cell size. The filling factor is kept constant ($f = 0.64$) for the circle and the square, this was however not possible for the cross as its geometry doesn't allow it. The geometry was therefore set to have $1\mu m$ left on each side of the cross for manufacturing process reasons, leading to a filling factor of $f = 0.43$. The thickness of the layer is set to $h = 1\mu m$.

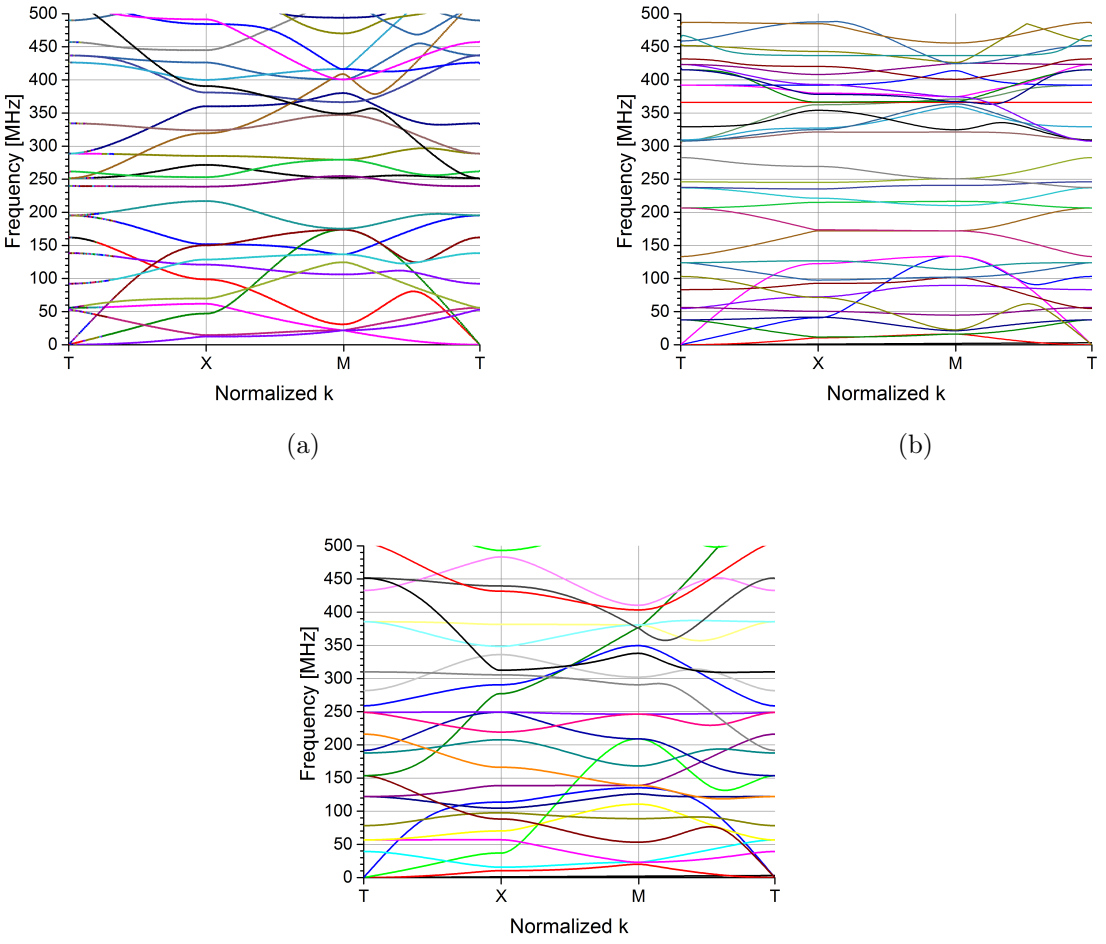

(a) (b)

(c)

Figure 25: Band diagram of the three different geometries for the same unit cell size $a = 17\mu m$: a) circle unit cell b) cross unit cell c) square unit cell

Some characteristic shape of the bands at low frequencies are found for the three geometries and we can suppose these modes are specific to the square arrangement of the unit

cell.
A band gap is present for both the circle and the square unit cells, but the center frequency is situated at 230MHz for the circle and at 290MHz for the crosses. As the unit cell size is the same, this is probably due to the difference in the geometry and filling factor, which is coherent with Figure 8a that predicts a lowering in the center frequency of the band gap with an increase in the filling factor. No band gap is present for the square unit cell, with a very small chance of finding a deaf band gap as a consequent number of modes are covering a very wide range of frequencies. Simulations have been further performed for this geometry and a larger filling factor ($f = 0.78$) but this did not lead to an opening of any band gap and the same global shape with modes covering a wide range of frequencies was found.
The band diagram of the cross shape is promising in terms of deaf band gap as the bands are very flat in the140-300MHz frequency range. It is however difficult to define the nature of the modes from the mode shape for this geometry and some modes seemed to be of mixed nature (both transverse and longitudinal but in different directions).

7 Transmission quantification

The band diagram analysis gives precious informations about the behavior of the complete band gap, but it is more uncertain about predicting deaf band gaps and doesn't allow to determine to which *attenuation* a certain number of repetitions would lead to in terms of decibels. These are informations that a quantification set-up can give. Quantification simulations however have the disadvantage of lasting much longer than band diagram ones, this is why a first targeting with band diagrams is very useful.

7.1 Model

The quantification set-up is shown on Figure 26 and is composed of the following elements:

1. The excitation source simulates the resonator's motion: a prescribed displacement of $1\mu m$ is set on two faces at a certain frequency, each face moving out of phase from each other. The resonator's motion is mainly in the y direction, but the Poisson ratio coupling also induces a movement in the x and z directions. All three excitations have been simulated for each configuration.

2. The phononic crystal is placed on the substrate after the supporting beam. The same number of repetitions (N) is set in each direction from the attachment point: there is therefore twice as many repetition in y than in x.

3. The probe is a vertical surface surrounding the PnC, its total displacement is extracted.

4. Perfectly matched layers (PML) are placed around the whole structure. They are dimensioned such that they absorb all the energy of the waves impinging and therefore prevent the reflection of the waves at the boundaries.

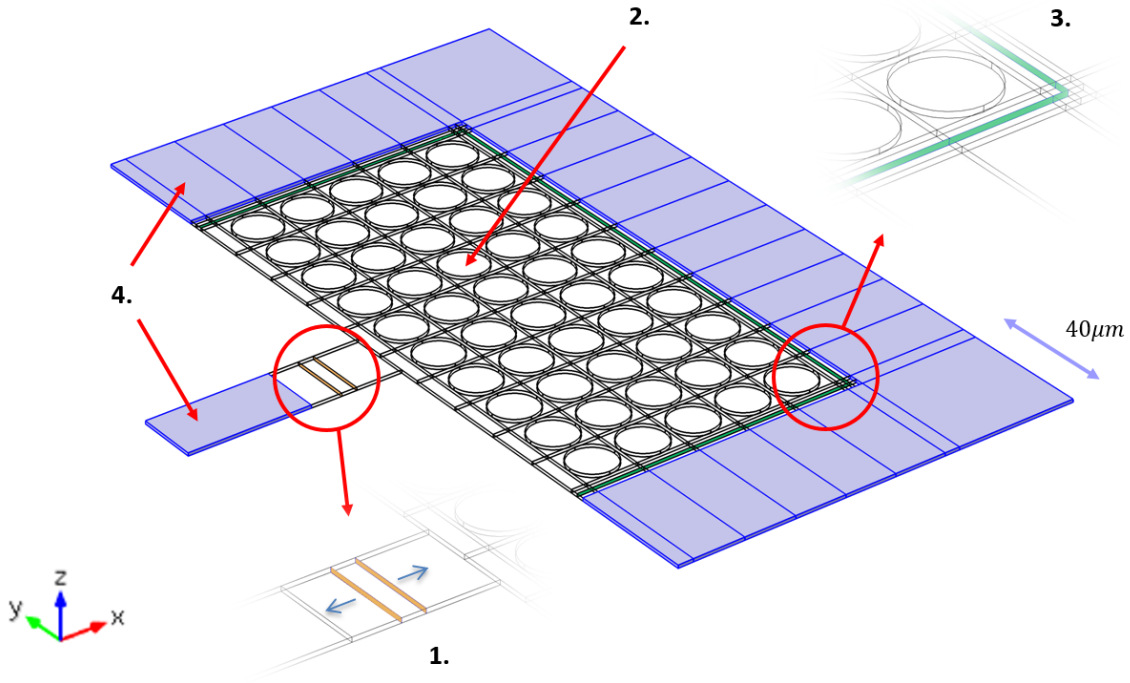

Figure 26: Quantification set-up: 1. Excitation source (x excitation shown here) 2. PnC 3. Probe 4. PML

The transmission in decibels is then given by the following formula:

$$T_{dB} = 10 \cdot log\left(\frac{u^2_{probe}}{u^2_{source}}\right) \tag{3}$$

u being the total displacement.

7.2 Geometry comparison

The transmission has been measured as a function of the frequency for the same unit cell size and same number of repetitions for the three different geometries in order to compare which one leads to a larger attenuation. The filling factors are obtained by setting the minimum distance between the side of the unit cell and the air fraction to be $1\mu m$ because of manufacturing limitation. The resulting graphs are shown on Figure 27.

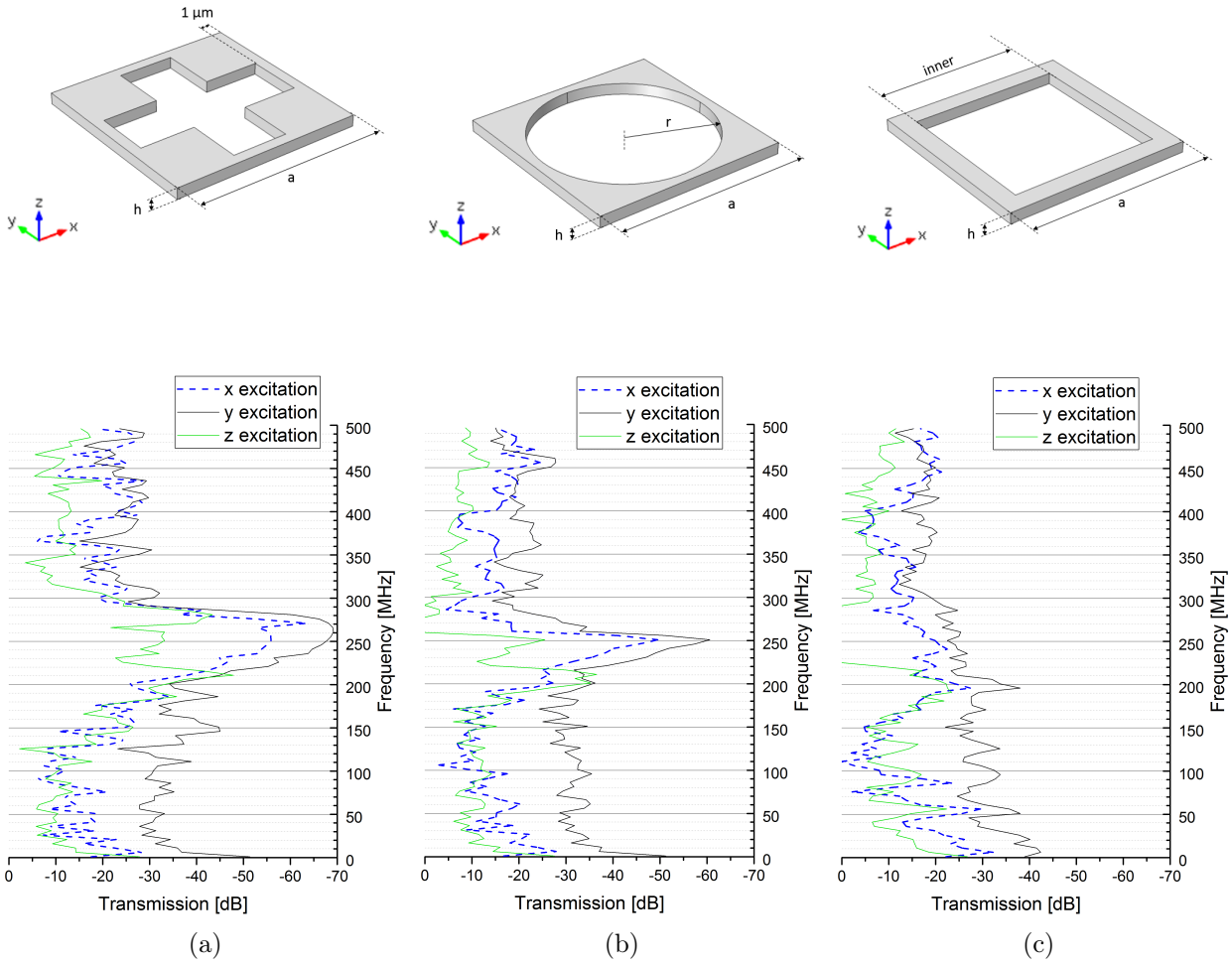

(a) (b) (c)

Figure 27: Transmission as a function of frequency for the three different geometries with $a = 17\mu m, h = 1\mu m, N = 5$: a) cross unit cel, $f = 0.43$ b) circle unit cell, $f = 0.61$ c) square unit cell, $f = 0.78$

The first conclusion that can be drawn from these graphs is that the square unit cell leads to nearly no dip in transmission, which confirms the supposition made from the band diagrams. A small dip in transmission of -40dB is observed at 200MHz for all the three geometries. A much larger dip in transmission is observed around 250MHz for the cross and the circle unit cells. The dip is a bit larger for excitations in all the three directions in the case of the cross unit cell than for the circle unit cell despite the smaller filling factor. More importantly: the peak of attenuation is wider for the x and y excitations in the case of the cross unit cell, which makes this geometry more interesting for a future integratio: indeed the material properties will depend on fabrication process (due to intrinsic stress for example) and may differ from the simulation, which means that the peak of attenuation can be shifted in frequency. Therefore a wide peak of attenuation means that the frequency of operation of the CMR will be more likely to lie in the PnC's freqeuncy range of attenuation. The next sets of simulation will therefore focus on this geometry.

7.2.1 Comparison between the band diagram and transmission graph for a circle unit cell

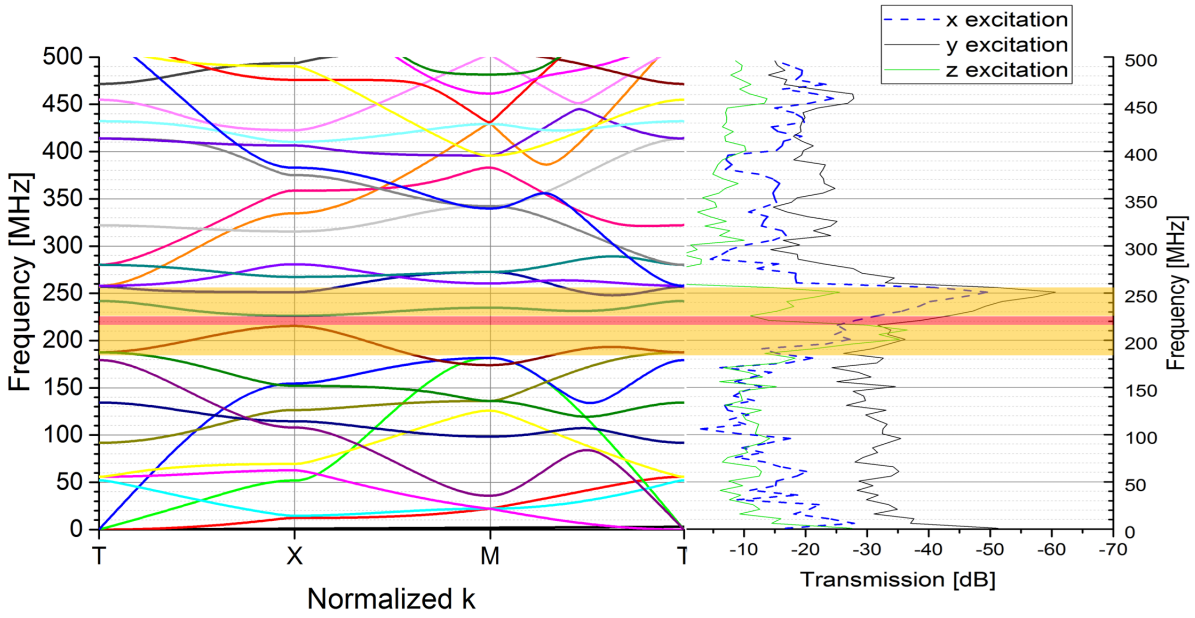

Figure 28: Comparison between the band diagram and transmission graph for a circle unit cell with $a = 17\mu m, f = 0.61, h = 1\mu m, N = 5$

The red and yellow shaded area are respectively the complete and supposed deaf band gap. As the largest attenuation is very likely to be due to the complete band gap, a shift in frequency is observed between the position of the complete band gap as predicted by the band diagram and the observed peak in transmission. This effect is probably due to the fact that the band diagram is obtained by imposing a condition at the boundaries that assumes an infinite number of repetitions of the unit cell in these directions, which is obviously not the case in this case.
By comparing the transverse mode situated below the complete band gap previously supposed as not carrying energy with the corresponding value of the transmission, it can be seen that this mode is associated with a small attenuation in transmission but that it is still carrying a consequent amount of energy. By comparing the modes situated above the band gap that were previously supposed as deaf with the corresponding value of the transmission, it is observed that these modes carry a consequent amount of energy and do not lead to any attenuation. This emphasizes the limitations of the band diagram analysis.

7.2.2 Comparison between the band diagram and transmission graph for a cross unit cell

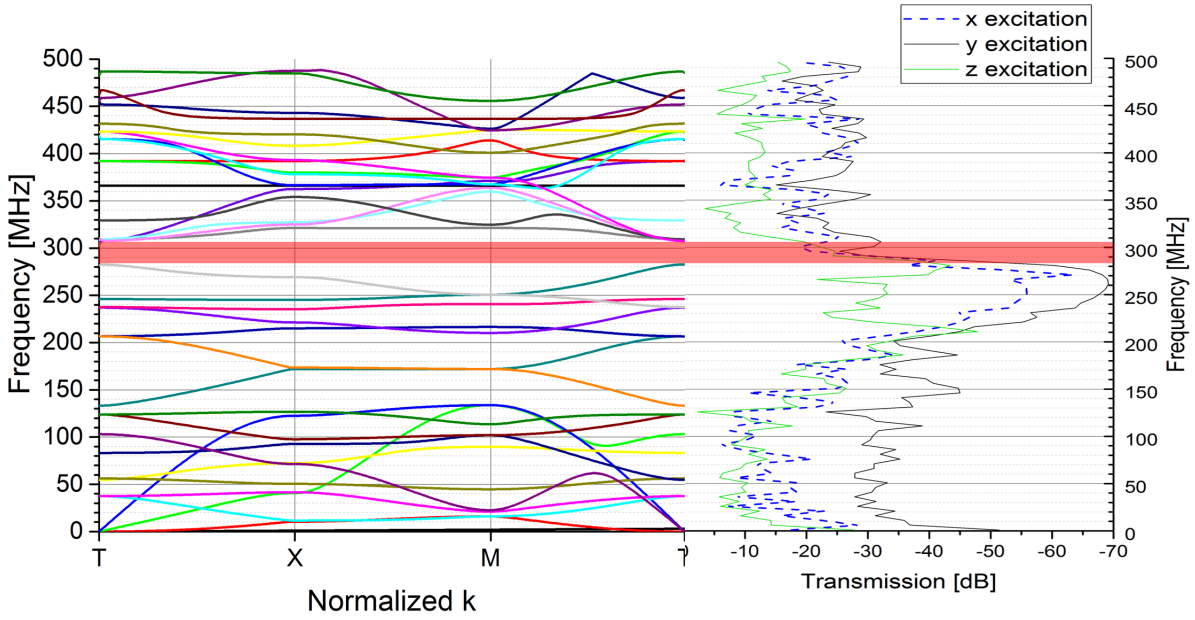

Figure 29: Comparison between the band diagram and transmission graph for a cross unit cell $a = 17\mu m, f = 0.43, h = 1\mu m, N = 5$

In this case the largest dip in transmission is shifted compared to the complete band gap observed on the band diagram, but this time the largest dip in transmission happen for a lower frequency than what was predicted by the band diagram whereas an up shift was observed for the circle unit cell case. The reason for the shift is probably the same than what was supposed for the circle, but the reason for the direction of the shift is unknown. A step by step increase in transmission is observed for both x and y excitations when going down in frequency from largest dip in transmission, which can lead to the following hypothesis:

- The grey and petrol blue bands are modes that don't carry much energy but still carry more energy in the x direction than the y direction
- The pink band and lower bands are associated with modes that carry energy

7.3 Number of repetition comparison

It is interesting to know how the attenuation is evolving with the number of repetitions as the attenuation it is directly linked to the quality factor. The transmission simulation has therefore been performed on PnCs composed of a cross unit cell for $N = 3, 5, 10$.

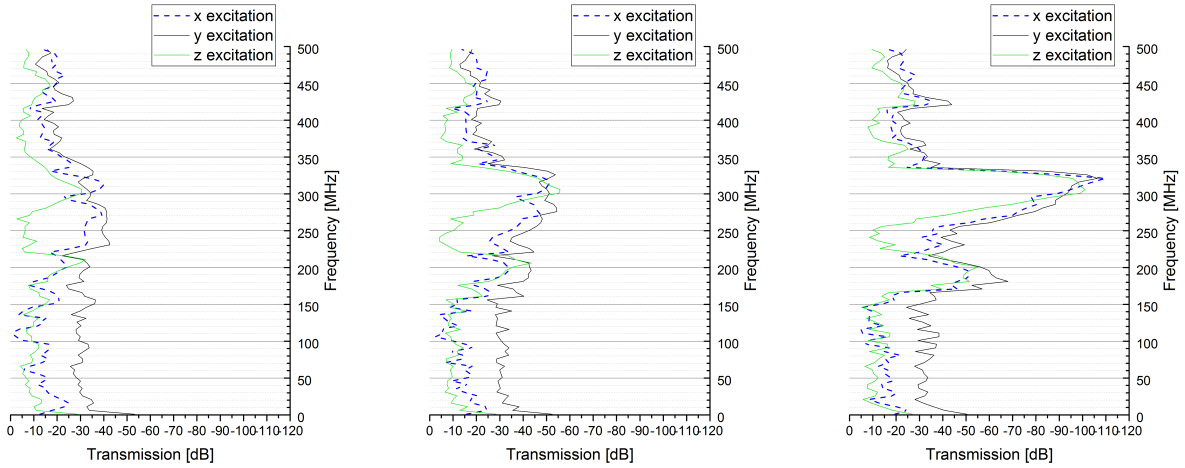

(a) (b) (c)

Figure 30: Transmission as a function of the number of repetition for a cross unit cell with $a = 14.5\mu m, h = 1\mu m, f = 0.41$: a) N=3 b) N=5 c) N=10

As expected the attenuation is larger with an increase in the number of repetitions with nearly no attenuation for $N = 3$. Furthermore, the attenuation of the major dip in transmission fits well to the following linear approximation:

$$T_{dB} = -11 \cdot N$$

A slight up shift in the position of the peak is observed when increasing the number of repetitions for the x excitation, whereas a down shift of the peak is observed for the y excitation, which confirms the hypothesis made previously: the difference between the frequency of maximum attenuation and the frequency of the band gap is due to the number of repetitions. Also a second dip in transmission appears for $N = 10$ around 190 MHz.

7.3.1 Comparison between the band diagram and transmission graph for a cross unit cell

No band gap is found on the band diagram of a cross unit cell with $a = 17\mu m, f = 0.41, h = 1\mu m$, it is therefore difficult to say which bands lead to the maximum dip in transmission. However, when assuming that the same shift in frequency between band diagram and transmission graph happen for the same geometry and number of repetitions but different unit cell sizes (a shift of 20 MHz has been observed on Figure 29), a certain number of deductions can be drawn from the comparison between band diagram and transmission graph (Figure 31):

- Purple and petrol blue bands (between lines 1. and 2.) are deaf modes
- Pink band (line 2.) is not a deaf mode
- Purple band (between lines 2. and 3.) is a deaf mode

- The region between lines 4. and 5. is what will becom the second dip in transmission for a larger number of repetitions. Probably that the colors are misleading here and that the petrol blue band and orange band mix at the point of intersection: what is between lines 4. and 5. would therefore be a single mode that doesn't carry much energy whereas bands between lines 3. and 4. are more likely to be excited by the resonator's motion.

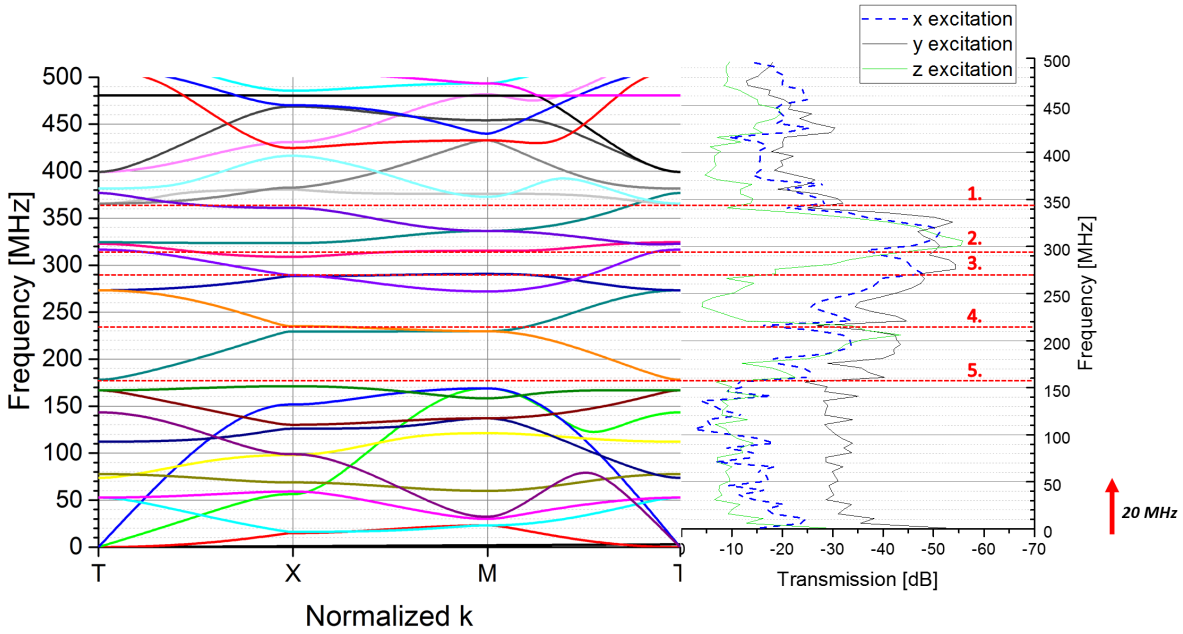

Figure 31: Comparison between the band diagram and transmission graph for a cross unit cell $a = 14.5\mu m, f = 0.41, h = 1\mu m, N = 5$ with a shift in frequency of $20MHz$

7.4 Material comparison

As the CMR is actuated by electrodes, a 100 nm platinum layer is deposited on both sides of the $1\mu m$ AlN layer. At the this time, it is not yet known if both Pt layers can be patterned or only the one situated on top. A pattering could allow to free the PnC from the Pt layer by deviating the metal track on the side of the PnC as done for example by Zhu & Lee [13] on Figure 18a. It is interesting to explore the effect that such layers have on the behavior of the PnC. Band diagram and quantification simulations have been performed for a cross unit cell with: AlN only, AlN and Pt on one side, and AlN sandwiched between two Pt layers. The hypothesis made was that such a thin layer wouldn't have much influence on the behavior of the PnC.

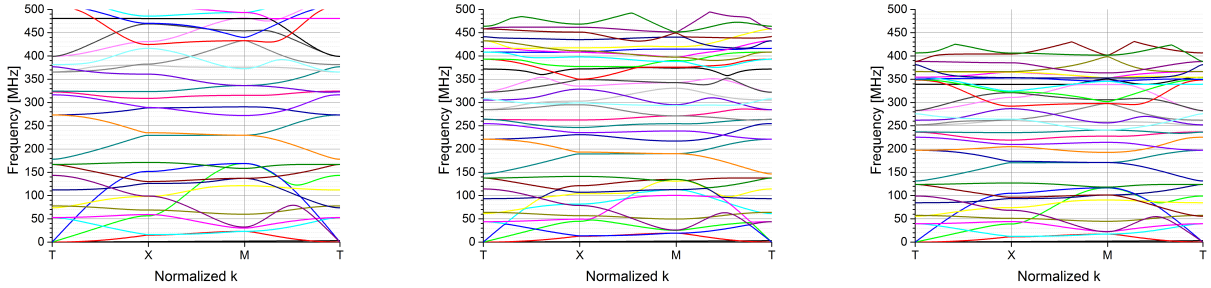

(a) (b) (c)

Figure 32: Band diagram as a function of the material composition for a cross unit cell with $a = 14.5\mu m, h_{AlN} = 1\mu m, h_{Pt} = 100nm, f = 0.41$: a) AlN b) AlN + Pt on top c) AlN + Pt top and bottom

From the band diagram it can be seen that the addition of Pt shrinks the band diagram, the global shape is however conserved for all three graphs. The same conclusion can be drawn from this comparison than the ones made for section 6.2: since Pt has smaller $\frac{E}{\rho}$ and $\frac{G}{\rho}$ ratios this induces a reduction of the effective wave velocity in the medium for the same mode and same wave vector leading to a lowering of the bands on the band diagram as the Pt layer content increases. It can be expected that the transmission graphs will follow the same behavior: a global shape conserved with a shrinkage in frequency as the Pt content increases. Figure 33 gives the graphs resulting from the transmission simulations.

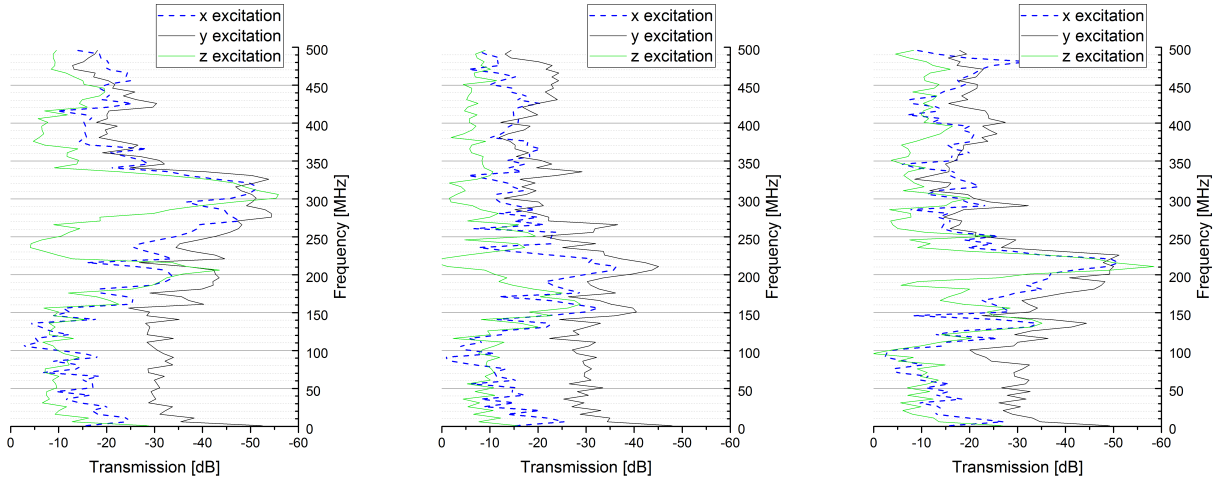

(a) AlN (b) AlN + Pt on top (c) AlN + Pt top and bottom

Figure 33: Transmission as a function of the material composition for a cross unit cell with $a = 14.5\mu m, h_{AlN} = 1\mu m, h_{Pt} = 100nm, f = 0.41$ and $N = 5$

Figure 33c effectively has the shape of a compressed version of 33a, with a sharper dip in transmission and at a lower frequency for the unit cell containing Pt and approximately

the same minimum in transmission value for both cases. Surprisingly, the structure containing a Pt layer on one side only leads to a much lower, nearly not distinguishable dip in transmission. A pronounced difference in the behavior of the transmission is observed especially for a z excitation, which leads to the supposition that the asymmetry in the z direction induced by the presence of the Pt layer only on one side allows waves to travel more easily through the structure, and maybe more specifically surface acoustic waves (SAW).
A structure formed by Pt only on one side is therefore not interesting for waves reflection. AlN only would be more interesting because it has a broader peak of attenuation than AlN and two Pt layers, but this latter has a peak of attenuation situated lower in frequency which is interesting because it would require a smaller unit cell size than the AlN case for a peak situated at the same frequency. This would mean that a larger number of repetitions could be integrated on a given surface and thus a larger attenuation could be achieved. But this is true as long as the peak of attenuation fits perfectly the frequency of operation of the resonator which is not guaranteed because of the shift in frequency of the real structure compared to the simulations for the reasons mentionned earlier.

8 Conclusion

A model has been validated using a FEM commercial software for both 1D and 2D PnCs. The behavior of the band diagram has been studied as a function of unit cell size, filling factor, material and geometry, whereas the behavior of the transmission graphs has been studied as a function of geometry, number of repetition and material composition. Furthermore, comparisons of the band diagram and transmission graphs have been performed leading to some suppositions about the nature of the modes and the observation of a shift in the frequency of the band gap due to the number of repetitions of the unit cell.
From the study of the evolution of the band diagram as a function of the unit cell size, it has been observed that a linear approximation can predict with a good precision the position of the band gap. It also has been found that determining if a mode is likely to be excited by a CMR is an information that is more reliably given by comparison of the transmission graph and the band diagram than by the mode shape.
From transmission simulations performed on cross, circle and square unit cells, it has been found that the cross unit cell was leading to a thicker peak and a larger attenuation than the other geometries, which makes it preferred for a future integration. It also has been found that the attenuation fits well to a linear dependence on the number of repetitions. A surprising result has been observed from comparing the transmission for PnCs composed of different materials, leading to the conclusion that the presence of a 100nm Pt layer on one side only disturbs the reflection properties of a PnC. An integration with no Pt or Pt on both sides of the AlN layer is therefore preferred. The first structure has the advantage of having a broader peak of attenuation, whereas the second structure can be more compact for the same attenuation.
Abdelkrim & Adibi [1] report that an hexagonal lattice arrangement of a circle unit cell leads to an increase in the band gap width compared to its square-lattice equivalent. A further study on the behavior of a PnC composed of cross unit cells arranged in an

hexagonal fashion could therefore be interesting . A tapered evolution of the unit cell size for a cross unit cell could also be interesting as it has been shown by Wang et al. [11] that a tapered circle unit cell PnC increases the reflection of waves and thus the Q factor of the resonator.
It is important to emphasize that all simulations done in this work are approximations and that intrinsic stress induced by the fabrication process for example can modify the velocity of propagation of the waves in the structure, inducing a shift in the peak of attenuation of a PnC. As this latter is very sharp in the case of a PnC formed by AlN sandwiched between two Pt layers, it would be interesting to measure the Q factor of resonators whose anchors are structured in PnCs of different unit cell sizes close to the one predicted by simulations in order to avoid a PnC whose frequency of minimum transmission is shifted compared to the working frequency of the resonator.

References

[1] Khelif Abdelkrim and Adibi Ali. *Phononic Crystals, Fundamentals and Applications.* Springer-Verlag New York, 1 edition, 2016.

[2] B. Bahr, R. Marathe, and D. Weinstein. Theory and Design of Phononic Crystals for Unreleased CMOS-MEMS Resonant Body Transistors. *Journal of Microelectromechanical Systems*, 24(5):1520–1533, October 2015.

[3] Taras Gorishnyy, Martin Maldovan, Chaitanya Ullal, and Edwin Thomas. Sound ideas. *Physics World*, 18(12):24, 2005.

[4] F.-C. Hsu, J.-C. Hsu, T.-C. Huang, C.-H. Wang, and P. Chang. Design of lossless anchors for microacoustic-wave resonators utilizing phononic crystal strips. *Applied Physics Letters*, 98(14):143505, April 2011.

[5] Feng-Chia Hsu, Chiung-I Lee, Jin-Chen Hsu, Tsun-Che Huang, Chin-Hung Wang, and Pin Chang. Acoustic band gaps in phononic crystal strip waveguides. *Applied Physics Letters*, 96(5), 2010.

[6] N. K. Kuo and G. Piazza. 1 GHZ phononic band gap structure in air/aluminum nitride for symmetric lamb waves. *Micro Electro Mechanical Systems (MEMS), 2011 IEEE 24th International Conference on*, pages 740–743, January 2011.

[7] N.K. Kuo and G. Piazza. Fractal phononic crystals in aluminum nitride: An approach to ultra high frequency bandgaps. *Applied Physics Letters*, 99(16), 2011.

[8] N.K. Kuo, C. Zuo, and G. Piazza. Microscale inverse acoustic band gap structure in aluminum nitride. *Applied Physics Letters*, 95(9), 2009.

[9] C.M. Lin, J.C. Hsu, D.G. Senesky, and A.P. Pisano. Anchor loss reduction in ALN Lamb wave resonators using phononic crystal strip tethers. *2014 IEEE International Frequency Control Symposium (FCS)*, pages 1–5, May 2014.

[10] J. Segovia-Fernandez, M. Cremonesi, C. Cassella, A. Frangi, and G. Piazza. Anchor Losses in AlN Contour Mode Resonators. *Journal of Microelectromechanical Systems*, 24(2):265–275, April 2015.

[11] S. Wang, L. C. Popa, and D. Weinstein. Tapered Phononic Crystal sawresonator in GaN. In *2015 28th IEEE International Conference on Micro Electro Mechanical Systems (MEMS)*, pages 1028–1031, January 2015.

[12] S. Wang, L.C. Popa, and D. Weinstein. GaN MEMS resonator using a folded phononic crystal structure.

[13] H. Zhu and J.E. Y. Lee. AlN piezoelectric on silicon MEMS resonator with boosted Q using planar patterned phononic crystals on anchors. *2015 28th IEEE International Conference on Micro Electro Mechanical Systems (MEMS)*, pages 797–800, January 2015.

[14] M. Ziaei-Moayyed, M. F. Su, C. Reinke, I. F. El-Kady, and R. H. Olsson. Silicon carbide phononic crystal cavities for micromechanical resonators. *Micro Electro Mechanical Systems (MEMS), 2011 IEEE 24th International Conference on*, pages 1377–1381, January 2011.